Disordered Triblock Polymers for Nanoporous Materials with Tunable Surface Properties for Ultrafiltration Applications

*Wui Yarn Chan and Marc A. Hillmyer**

Department of Chemistry, University of Minnesota, Minneapolis, Minnesota 55455

KEYWORDS

Triblock polymer, self-assembly, bicontinuous, fluctuating disordered state, selective etching, solution casting, hydrophilic ultrafiltration membranes

ABSTRACT

Triblock polymers trapped in the fluctuating disordered state were investigated as precursors to nanoporous ultrafiltration membranes. The triblocks explored are poly(lactide)-*b*-poly(oligoethylene glycol methyl ether methacrylate)-*b*-poly(styrene-*s*-methyl methacrylate) (PLA-POEGMA-PSMMA), where PLA is the etchable pore-forming block, POEGMA is the hydrophilic pore-lining block, and PSMMA is the matrix block. Bicontinuous microphase separated domains were obtained thermally by heating the polymer melt above the order-disorder transition temperature (T_{ODT}) followed by quenching below the glass transition temperature (T_g), or isothermally by spin coating the block polymer solution at ambient conditions. POEGMA is miscible with PLA but not PSMMA, and should therefore co-localize with PLA and be exposed on pore surfaces after selective PLA etching. The triblock polymers have similar ODT behavior as diblock polymers, and the presence of an accessible T_{ODT} in the melt depends strongly on the segregation strength $\chi_{PLA\text{-}PSMMA}N$. Composite membranes with block polymer selective layers were prepared by spin coating the triblock polymer onto water filled Nylon membranes, where rapid solvent evaporation enabled the block polymer to be vitrified in the disordered state. The resulting membranes have uniform surface pores, high permeabilities, small improvements in surface hydrophilicity, and the approach may be applied to target other surface functionalities.

TOC Graphic

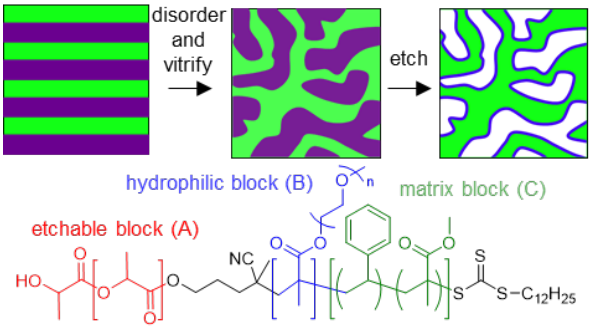
disorder
and
vitrify
etch
hydrophilic block (B)
matrix block (C)
etchable block (A)
HO
O
O
O
NC
O
O
O
O
n
S
S
S–C12H25

INTRODUCTION

Ultrafiltration (UF) membranes are used to perform separations in many areas, including biomedical applications, water purification, and industrial processes. Conventional UF membranes are commonly prepared using phase separation techniques such as non-solvent induced phase separation (NIPS) with homopolymers.[1] Although high porosity and high permeability can be achieved in such membranes, pore size distributions are generally wide, limiting membrane size selectivities.[2] Additionally, targeting specific surface properties often requires addition of additives into membrane casting solutions, or treatment and chemical functionalization post membrane formation.[3-4]

Microphase separated block polymers have emerged as attractive membrane materials as they provide improvements in size selectivity and tailorable surface chemistries.[2, 5-7] Block polymers with two or more incompatible segments can self-assemble into well-organized domains on the order of tens of nanometers, which can template or be converted into highly uniform pores. Nanopores can be generated in the block polymer material by selective removal of one of the domains through chemical etching or leaching, or by selectively swelling of one of the domains.[8-14] Evaporation induced self-assembly followed by non-solvent induced phase separation (SNIPS) has also been demonstrated as a successful strategy, where the packing of micelles on the surface during solvent evaporation and subsequent precipitation leads to asymmetric structures with ordered cylindrical channels on top of highly porous sublayers.[14-16] These nearly isoporous membranes can facilitate the separation of solutes with size differences smaller than previously achievable for conventional NIPS membranes.[2] Additionally, amphiphilic block polymers, which are commonly used in the selective swelling or SNIPS

strategies, have pores that are inherently hydrophilic and may therefore impart fouling resistance to the membranes.[17]

The ability to target specific pore surface properties is important in the design of high performance (e.g., low fouling) membranes and in enabling separations beyond size exclusion. Judicious selection of monomers can enable desired functional moieties to be installed on pore walls for tuning surface properties or performing pore wall functionalization chemistries. One such strategy involves incorporating a functional block in the copolymer precursor that is exposed on the pore surface, for example, in AB/AC diblock polymer blends where A is the matrix block and B and C are the pore-forming and pore-lining blocks respectively.[18] Functional membranes have also been prepared with multiblock polymers, such as ABC triblock polymers that form core-shell cylindrical morphologies with the B midblock lining pores after selective removal of an end block.[19-20] In addition, pore wall-lining blocks amenable to post-membrane formation functionalization chemistries can be selected, which allows membrane surfaces to be modified for additional selectivity and affinity-based separations.[20-22]

Ordered morphologies with at least one domain that percolate the entire membrane thickness are required for membrane applications, and bicontinuous domains are attractive because the inherent connectivity eliminates the need for additional domain alignment steps. The fluctuating disordered state has therefore received attention as membrane materials due to its bicontinuous network morphology. At temperatures far above the order-disorder transition temperature (T_{ODT}) of block polymers, phase mixing occurs and homogeneous melts form due in part to the significant entropic penalty of chain stretching necessary in ordered phases. However, in the vicinity of the T_{ODT}, fluctuation effects become important, and block polymers can remain locally microphase separated despite having a loss of long-range correlations. While the

interfacial curvature is altered for the bicontinuous disordered structure, the composition profile or domain purity has been shown to remain unaffected near the lamellar to disorder transition.[23] We have previously demonstrated strategies to prepare nanoporous materials from fluctuating disordered block polymers, where diblock polymers slightly above the T_{ODT} were either crosslinked or vitrified by rapid quenching below the glass transition temperature (T_g) to fix or freeze the material in the disordered state.[24-27] Subsequent removal of the etchable domain in the diblock polymers resulted in isoporous membranes with a continuous pore structure.

In this work, we investigate the ODT behavior of ABC triblock polymers and explore the use of disordered triblock polymers for the preparation of isoporous membranes, where the midblock allows surface properties to be tailored. Inspired by previous work with roughly symmetrical poly(lactide)-*b*-poly(styrene-*s*-methyl methacrylate) (PLA-PSMMA),[24] with PLA as the etchable domain and PSMMA as the matrix block, we prepared poly(lactide)-*b*-poly(oligoethylene glycol methyl ether methacrylate)-*b*-poly(styrene-*s*-methyl methacrylate) triblock polymers (PLA-POEGMA-PSMMA). Since PLA is miscible with PMMA but not PS, the percent styrene incorporated in the matrix block allows the interaction parameter, χ, to be tuned such that T_{ODT} falls within accessible temperature ranges for polymer melts. POEGMA was selected as the model midblock due to its hydrophilicity and the fouling resistant properties of PEG-based materials[28-30]. Upon etching, the POEGMA block exposed on pore walls is hypothesized to impart surface hydrophilicity to membranes. The triblock polymers were characterized by dynamic mechanical analysis and small angle x-ray scattering (SAXS). After selective removal of PLA, scanning electron microscopy (SEM) and nitrogen sorption were also performed on the nanoporous materials. Contact angle measurements and fouling studies were performed on Nylon membranes coated with the triblock polymers.

RESULTS AND DISCUSSION

ABC triblock polymers were designed for the preparation of nanoporous materials with hydrophilic pore walls, where a short pore-lining midblock serves as a handle for tuning surface properties and is flanked by a rigid matrix block and an etchable polyester pore-forming block. Poly(styrene-*s*-methyl methacrylate) (PSMMA) and poly(lactide) (PLA) were selected as the rigid matrix block the etchable block respectively, which were previously reported to form microphase separated nanostructures when the styrene content in the matrix block is sufficiently large.[24] As hydrophilic membrane surfaces are desirable for fouling resistance,[31] poly(oligo ethylene glycol methyl ether methacrylate) (POEGMA) was selected as the midblock. Bicontinuous domains were achieved by heating the ordered material above T_{ODT}, followed by vitrification by quenching below the T_g of the matrix block, using a similar strategy previously described for PLA-PSMMA diblock polymers.[24] In the fluctuating disordered state, composition fluctuations disrupt long range order, but locally, the composition profile across the interface of the microphase separated domains remains nearly identical to the ordered material.[32-33] Vitrification traps the material in the disordered and globally isotropic state, and selective removal of the three dimensionally connected PLA domains then enabled formation of percolating nanopores (Figure 1). The midblock, which is exposed on the pore surface upon selective removal of the PLA block, can therefore be used to impart surface hydrophilicity.

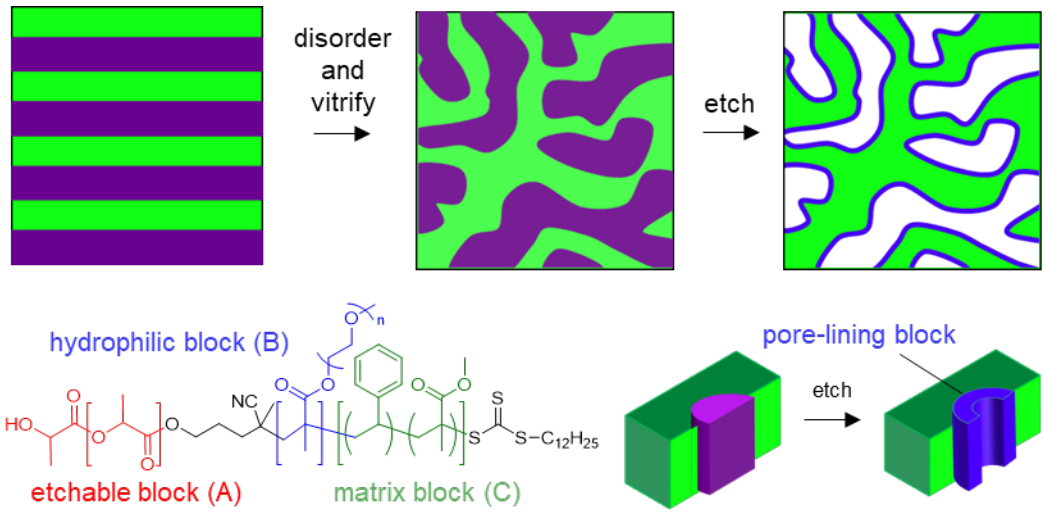

Figure 1. Disordered triblock polymer strategy for tuning pore wall properties, with PLA as the etchable pore-forming block, POEGMA as the hydrophilic block, and PSMMA as the matrix block. Nanopores were obtained by heating the block polymer above the order-disorder transition temperature, followed by vitrification and chemical etching. The hydrophilic POEGMA block co-localizes with PLA and is exposed on the pore surface upon sacrificial etching. For the POEGMA block, n = 4.5 on average.

The triblock polymers were synthesized by ring opening transesterification polymerization (ROTEP) of lactide with a hydroxyl terminated reversible addition fragmentation chain transfer (RAFT) agent as the initiator, followed by two successive RAFT polymerizations of OEGMA, and then of a mixture of styrene and methyl methacrylate. The OEGMA molar mass is 300 g/mol, corresponding to an average of 4.5 ethylene glycol units on the side chain. Molecular characteristics of diblock and triblock polymers and the naming conventions are given in Table 1, where the triblocks are named PLA-POEGMA$_m$-PSMMA, where m is the molar mass of the POEGMA midblock.

Table 1. Molecular characteristics of diblock and triblock polymers used in this study. Triblocks are labeled PLA-POEGMA$_m$-PSMMA, where m is the molar mass of the POEGMA midblock.

Sample ID	$M_{n,\,PLA}$[a] (kg/mol)	$M_{n,\,POEGMA}$[a] (kg/mol)	$M_{n,\,PSMMA}$[a] (kg/mol)	x_S (mol%)[b]	$Đ$[c]	T_{ODT} (°C)[d]
PLA-PSMMA	14.3		12	51	1.16	190
PLA-POEGMA$_{0.4k}$-PSMMA	14.3	0.4	12	48	1.17	190
PLA-POEGMA$_{2.9k}$-PSMMA	13.8	2.9	14	44	1.38	190
PLA-POEGMA$_{4.3k}$-PSMMA	13.8	4.3	14	37	1.27	160[e]
PLA-POEGMA$_{3.0k}$-PSMMA-L[g]	20.4	3.0	25	25	1.38	190
PLA-POEGMA$_{3.5k}$-PS	12.8	3.5	18	100	1.12	-[f]

[a]Number-average molar mass estimated from ^{1}H NMR spectroscopy. [b]Mole percent styrene in the PSMMA matrix block, estimated from ^{1}H NMR spectroscopy. [c]Molar mass dispersity, determined from SEC-MALLS. [d]Order-disorder transition temperature determined using variable temperature SAXS unless otherwise stated. T_{ODT} estimated from the change in slope in the $I(q^*)^{-1}$ vs T^{-1} plot, with an uncertainty of ±10 °C. [e]T_{ODT} determined using dynamic mechanical analysis, where the change in the slope of G' in a dynamic temperature sweep experiment indicates the transition. [f]ODT not detected, T_{ODT} above 220 °C. [g]Triblock with similar midblock molar mass as PLA-POEGMA$_{2.9k}$-PSMMA, but with larger end blocks.

As POEGMA is anticipated to be more compatible with PLA than the matrix, the midblock is likely co-localized in the etchable PLA domains. To assess this expectation, we performed differential scanning calorimetry (DSC) experiments using solution blended PLA and POEGMA homopolymers. DSC thermograms (Figure 2a) show the presence of only one T_g for the 23 wt% POEGMA blend, suggesting that the blend forms a homogeneous mixture. While the T_g corresponding to the PLA rich phase was not detected for the blend with the highest POEGMA content (91 wt%), at 50 wt% and 73 wt% POEGMA loading, the blends exhibit two T_g's, one very close to the homopolymer POEGMA T_g at –57 °C, and another between the T_g of POEGMA and PLA, suggesting that the blends phase separated into a relatively pure POEGMA phase and a mixed POEGMA/PLA phase. This composition-dependent miscibility is analogous to the behavior of PEG/PLA blends, where miscibility was observed for blends below a critical PEG concentration (~20 wt% for 10 kg/mol PEG), above which the segregation of a pure PEG

phase occurs.[34-35] Although two distinct T_g's observed for PEG/PLA with minimal crystallinity has been reported to be not a result of immiscibility but can be explained by the self-concentration model,[36] visual observations on the presence of distinct solid-like and liquid phases in the POEGMA/PLA blend at room temperature after drying the solution blended mixture suggested the formation of macrophase separated phases. As the mass fraction of POEGMA in the diblock precursors of materials listed Table 1 are small (0.03–0.37), PLA and POEGMA blocks are expected to form primarily miscible domains in the triblock polymers. In addition, the molar mass of POEGMA in triblocks (0.4–10.5 kg/mol) are smaller than the POEGMA homopolymer in the blend experiment (15.4 kg/mol), which may widen the composition window of miscibility.[34] In contrast, blends of POEGMA and PSMMA are opaque and show two distinct T_g's at -57 °C and 59 °C (Figure S6a), consistent with macrophase separation and incompatibility between the two blocks. Previous work on PLA-PSMMA diblock polymers has shown that when $x_S > 26\%$, two T_g's were observed (~50 °C and ~75-85 °C) for the microphase separated PLA and PSMMA domains.[24] PLA-POEGMA-PSMMA triblock polymers could therefore behave effectively as diblock polymers, with PLA-POEGMA as a single mixed block and PSMMA as the second block, where formation of microphase-separated structures depends largely on the styrene content in the PSMMA segment.

DSC thermograms for triblock PLA-POEGMA$_{2.9k}$-PSMMA and its diblock precursor PLA-POEGMA$_{2.9k}$ shown in Figure 2b suggest some degree of mixing in the triblock polymer. The diblock exhibits a single T_g at 27 °C, consistent with the formation of a single homogeneous phase. With the incorporation of the PSMMA block, only one T_g at 38 °C was observed. The increase in T_g for the triblock may be a result of some interfacial mixing with PSMMA. This is supported by the lack of a distinct PSMMA T_g, which is expected to be at around 83 °C from the

etched triblock after PLA hydrolysis. As the T_g of small POEGMA mass fractions can be difficult to detect, we cannot elminate the possibilty of decreases in PLA-POEGMA miscibility in the presence of PSMMA as a result of chain stretching effects when semicompatible diblocks are connected to incompatible end blocks. [37-38] However, since the POEGMA mass fraction is low, segregated pure POEGMA domains, if present along with the mixed PLA-POEGMA phase, will likely be small.

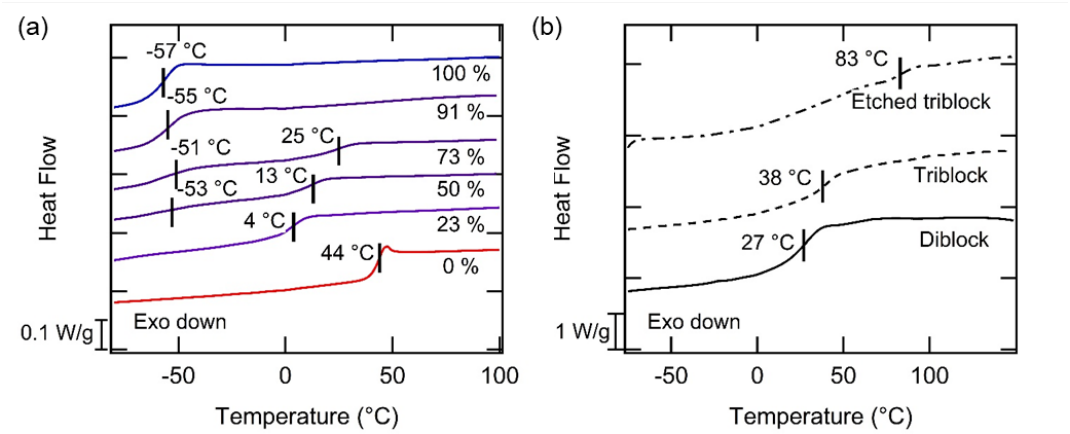

Figure 2. (a) DSC thermograms of POEGMA/PLA blends, where the molar masses of the PLA and POEGMA homopolymers are 12.6 kg/mol and 15.4 kg/mol respectively. Weight fractions of POEGMA are indicated on each trace. (b) DSC thermograms for PLA-POEGMA$_{2.9k}$-PSMMA (x_S=44 mol%), its diblock precursor PLA-POEGMA$_{2.9k}$, and the triblock material after selective removal of PLA. Thermograms for the second heating scan are shown, and the curves are vertically shifted for clarity. T_g's are indicated on each DSC trace.

Morphologies of the PLA-POEGMA-PSMMA triblock polymers were examined using variable temperature small-angle x-ray scattering (SAXS). Ordered structures were observed at low temperatures. Upon heating above the T_{ODT}, the scattering peaks broadened with increasing temperature, consistent with transitions to the fluctuating disordered state, and then eventually disappeared, consistent with the formation of mean field disordered melts. Figure 3 shows the diblock and a series of PLA-POEGMA-PSMMA triblocks with increasing midblock lengths that

have accessible T_{ODT}'s in the melt. Even though the DSC thermogram of PLA-POEGMA$_{2.9k}$-PSMMA (Figure 2b) suggests some phase mixing or diffuse interfaces, the SAXS results confirms that this triblock polymer is microphase separated (Figure 3c). The weak secondary scattering peaks for the triblock materials suggest that they have poor long range order, which prohibited unambiguous assignment of morphologies. The ratio of the first and second peaks for PLA-POEGMA$_{0.4k}$-PSMMA (Figure 3b) is $\sqrt{6}$:$\sqrt{8}$ and SEM images of the etched material provided some evidence for a network morphology below the T_{ODT} (Figure S7), but no conclusive morphological assignments are made. As the block polymer crosses the ODT, the primary scattering peak broadens and decreases in intensity as a result of the loss of long range order. The ODT is identified either by the onset of the peak broadening, or by the change in slope when the inverse intensity of the principal scattering peak $I(q^*)^{-1}$ is plotted against the inverse temperature T^{-1}.[24, 33] T_{ODT}'s were also estimated by rheological measurements. Precipitous drops in storage moduli (G') or changes in the slope of G' with increasing temperatures observed for PLA-POEGMA$_{0.4k}$-PSMMA and PLA-POEGMA$_{4.3k}$-PSMMA are attributed to ODT's,[23, 32] and the T_{ODT}'s obtained are generally in agreement with the SAXS measurements (Figures S8, 3). PLA-PSMMA and PLA-POEGMA$_{2.9k}$-PSMMA exhibited very small or undetectable changes in the slope of G' with temperature, which may be due to diffuse interfaces of weakly segregated block polymers as indicated by DSC results. Similar observations were also previously reported for PLA-PSMMA diblock polymers.[24]

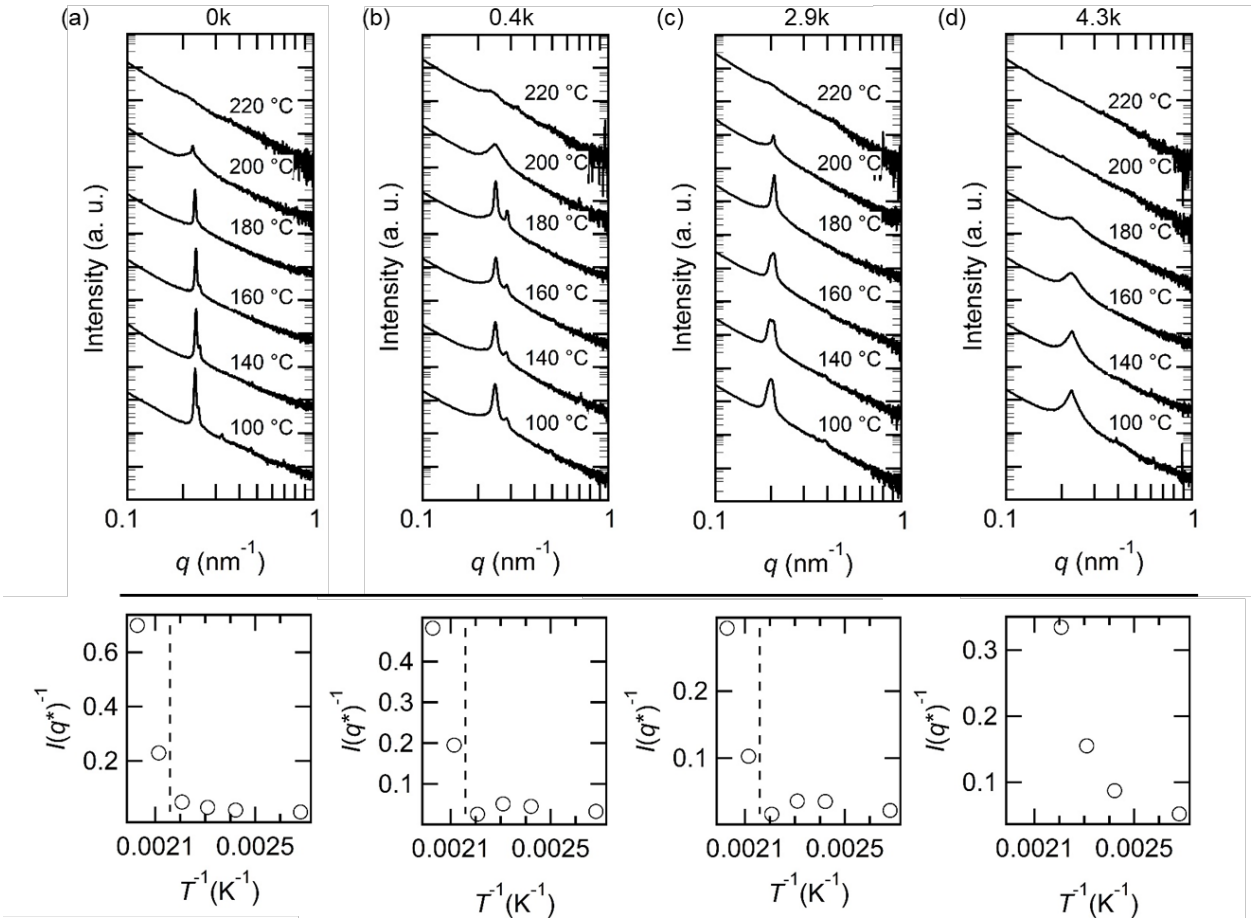

Figure 3. Variable temperature SAXS data on diblock and triblocks with varying midblock molar masses: (a) PLA-PSMMA, (b) PLA-POEGMA$_{0.4k}$-PSMMA, (c) PLA-POEGMA$_{2.9k}$-PSMMA, and (d) PLA-POEGMA$_{4.3k}$-PSMMA. POEGMA molar masses are indicated above SAXS plots. Top panel: 1D SAXS curves. Equilibration temperatures are indicated on each trace, and traces are vertically shifted for clarity. Bottom panel: inverse intensity of the principal scattering peak, $I(q^*)^{-1}$, plotted against inverse temperature, T^{-1}. Dashed lines indicate onset of a large change in slope, indicative of ODT. Change in slope not indicated in (d) due to the small number of data points.

Since the ABC triblock polymers in this study have compatible A and B blocks and incompatible A(B) and C blocks, the morphology and phase separation behavior potentially resembles that of diblock polymers, which are influenced by one interaction parameter, one independent volume fraction, and the degree of polymerization. For further investigation, triblocks with varying volume fractions f_{PLA} and f_{PSMMA}, molar mass, and styrene content were

synthesized (Table S1). Each data point in Figure 4 represents a triblock and is plotted according to the total polymer molar mass ($M_{n,\,triblock}$), mole percent styrene in the matrix block (x_S), and volume fraction of PSMMA (f_{PSMMA}) . Samples with accessible ODT in the temperature range 100–220 °C as measured by variable temperature SAXS are shown in black, while those that are disordered at 100 °C or have ODTs above 220 °C are shown in blue and red, respectively. Here, the most important parameters determining the presence of an accessible ODT in the melt are $M_{n,\,triblock}$ and x_S, which can be captured in the segregation strength $\chi_{PLA\text{-}PSMMA}N$ where $\chi_{PLA\text{-}PSMMA}$ is the interaction parameter between the two end blocks and N is the segment volume normalized degree of polymerization of all blocks. As PLA is miscible with PMMA but not PS, $\chi_{PLA\text{-}PSMMA}$ increases with styrene content in PSMMA and can be estimated using a binary interaction model:

$$\boldsymbol{\chi_{PLA-PSMMA} = (1 - w_S)\chi_{PLA-PMMA} + w_S\chi_{PLA-PS} + w_S(1 - w_S)\chi_{PS-PSMMA}} \quad \text{(eq. 1)}$$

where w_S is the weight fraction of styrene in PSMMA, $\chi(T) = A/T + B$, and the constants A and B for each pairwise interaction parameter were obtained from literature.[24, 39-40] Accordingly, the $\chi_{PLA\text{-}PSMMA}$ was calculated for each block polymer at 140 °C, and $(\chi_{PLA\text{-}PSMMA}N)_{140\,°C}$ was used as a proxy to evaluate end block compatibility (Tables S1, S2). Across a wide range of f_{POEGMA} (0.014–0.24), f_{POEGMA} has a negligible effect on the presence of accessible ODTs. On the other hand, triblocks with intermediate end block segregation strengths ($(\chi_{PLA\text{-}PSMMA}N)_{140\,°C}$ ~12–21) are noted to have accessible ODTs, while those with lower or higher $\chi_{PLA\text{-}PSMMA}N$ values are disordered or have T_{ODT}'s much higher than the accessible range. The triblocks therefore have similarities with diblock polymers, where PLA-POEGMA may act like one mixed block and segregation strength between the two end "blocks" strongly influences ordering. This is in contrast with triblock polymers with more chemically distinct A, B, and C blocks, where the

morphological diversity has been shown to be much richer than that of diblock polymers even in the case where the midblock B is small,[41] and can potentially even exhibit re-entrant ODT's.[42]

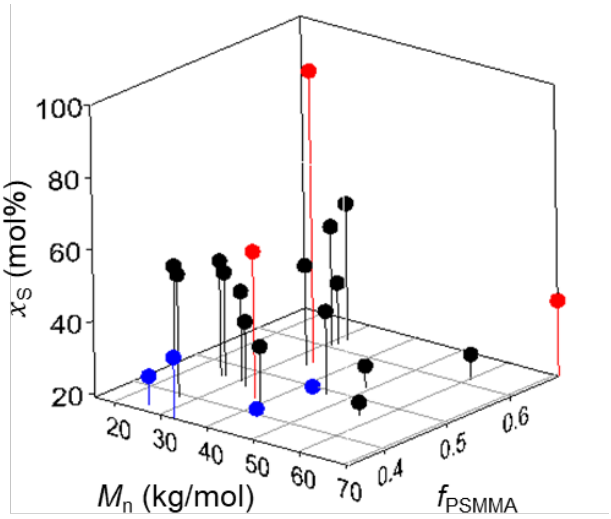

Figure 4. PLA-POEGMA-PSMMA triblock polymers (molecular details in Table S2) with varying volume fractions f_{PSMMA} and f_{POEGMA}, molar mass, and mole percent styrene in the matrix block (x_S). Polymers with accessible ODT in the range of 100 °C < T < 220 °C in black, polymers disordered at 100 °C in blue, and polymers with T_{ODT} > 220 °C in red.

Following chemical etching of block polymers vitrified in the fluctuating disordered state by sodium hydroxide solution, the PLA block was shown to be selectively hydrolyzed while the oligo(ethylene glycol) chains in POEGMA remain intact. ^{1}H NMR spectra of etched and unetched disordered PLA-POEGMA$_{2.9k}$-PSMMA in Figure 5 shows that after 2 days in 2M NaOH in 60/40 water/methanol (v/v), the PLA methine proton peak completely disappears, which is consistent with the bicontinuous morphology that allows percolating PLA domains to be accessible to the etching solution. On the other hand, the ratio of the POEGMA methylene protons to styrene aromatic protons remains the same. The molar mass of POEGMA homopolymer was also shown to be relatively unchanged after treatment in the etching solution (Figure S9). This is consistent

with previous observations in the literature, where the ester groups in polymerized POEGMA were shown to be resistant in aqueous NaOH solution, potentially due to a steric shielding effect.[43] NMR also shows that methyl protons of PMMA (2.1–3.8 ppm) were relatively unchanged after etching, potentially due to the inaccessibility of the bulk of the matrix domain to the etching solution. Incorporation of methanol in the etching solution was shown to speed etching, potentially due to improved wetting of PLA. Notably, presence of the POEGMA midblock slows down PLA hydrolysis, as shown in the large fraction of unetched PLA even after 5 days in 2M NaOH in water (Table S3), which is consistent with the mixed PLA-POEGMA domains as determined by DSC. All monolith etching was therefore performed in 60/40 water/methanol (v/v). However, pure methanol was noted to have detrimental effects on pore stability due to the slight plasticization of the uncrosslinked matrix. When etched triblock monoliths were soaked in methanol for extended periods of time, larger and more irregular pores were observed (Figure S10). Therefore, care was taken such that methanol concentration in all etching and wash solutions was limited to a maximum of 40 vol%. In addition, all dried materials for characterization were prepared by freeze drying to preserve pore structure, as hydrophilic membranes in particular can be prone to pore collapse due to high capillary pressures during evaporative drying.[44]

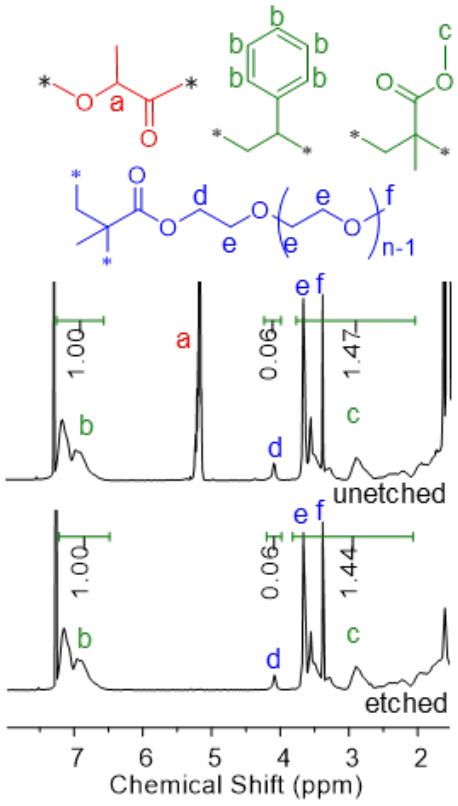

Figure 5. ^{1}H NMR spectra in $CDCl_3$ for triblock PLA-POEGMA$_{2.9k}$-PSMMA before and after selective etching. Peak integrals indicated for aromatic protons on styrene, methine proton on the PLA backbone, methylene protons next to the ester on POEGMA, and methyl protons on PMMA, which overlap with the methylene and methyl protons on POEGMA.

Nanoporous diblock and triblock monoliths were obtained after selective removal of the PLA domains, as confirmed by SAXS, nitrogen sorption, and SEM experiments. The fluctuating disordered morphology was trapped at room temperature by heating the block polymer melt to $T \approx T_{ODT}$+10 °C, followed by rapid quenching with liquid nitrogen.[24] SAXS of unetched monoliths show single broad peaks, consistent with the microphase separated disordered morphology also observed in the variable temperature SAXS experiments (Figure 3, 6). After etching, primary scattering peaks, q^*, were observed at the same position as those of the unetched precursors, along with the appearance of secondary peaks that are more pronounced due to the increased

scattering contrast from replacing the PLA domains with air.[40] The higher order reflections at $2q^*$ and $3q^*$ for the etched diblock (Figure 6a) suggests that this polymer had a lamellar ordering below the T_{ODT}, and some long range correlations persisted in the fluctuating disordered state. Appearances of additional peaks at $\sqrt{3}q^*$ for etched PLA-POEGMA$_{2.9k}$-PSMMA (Figure 6c) and at $2q^*$ for etched PLA-POEGMA$_{3.0k}$-PSMMA-L (Figure 6d) suggest lamellar or hexagonally packed cylinders in the triblock polymers below the T_{ODT}. Although a broad secondary peak was observed for etched PLA-POEGMA$_{0.4k}$-PSMMA (Figure 6b), it does not provide sufficient information for inferring the morphology below the T_{ODT}, as more complex network morphologies are possible (Figure 3b). Regardless of the equilibrium ordered morphology, bicontinuous networks were observed for monoliths vitrified in the disordered state and etched. The domain spacing, $D = 2\pi/q^*$, of the etched diblock and triblocks in Figure 5 range from 24–33 nm. Assuming that the volume fraction of the pores is equal to the volume fraction of PLA, the pore diameters estimated from SAXS measurements are 12–14 nm.

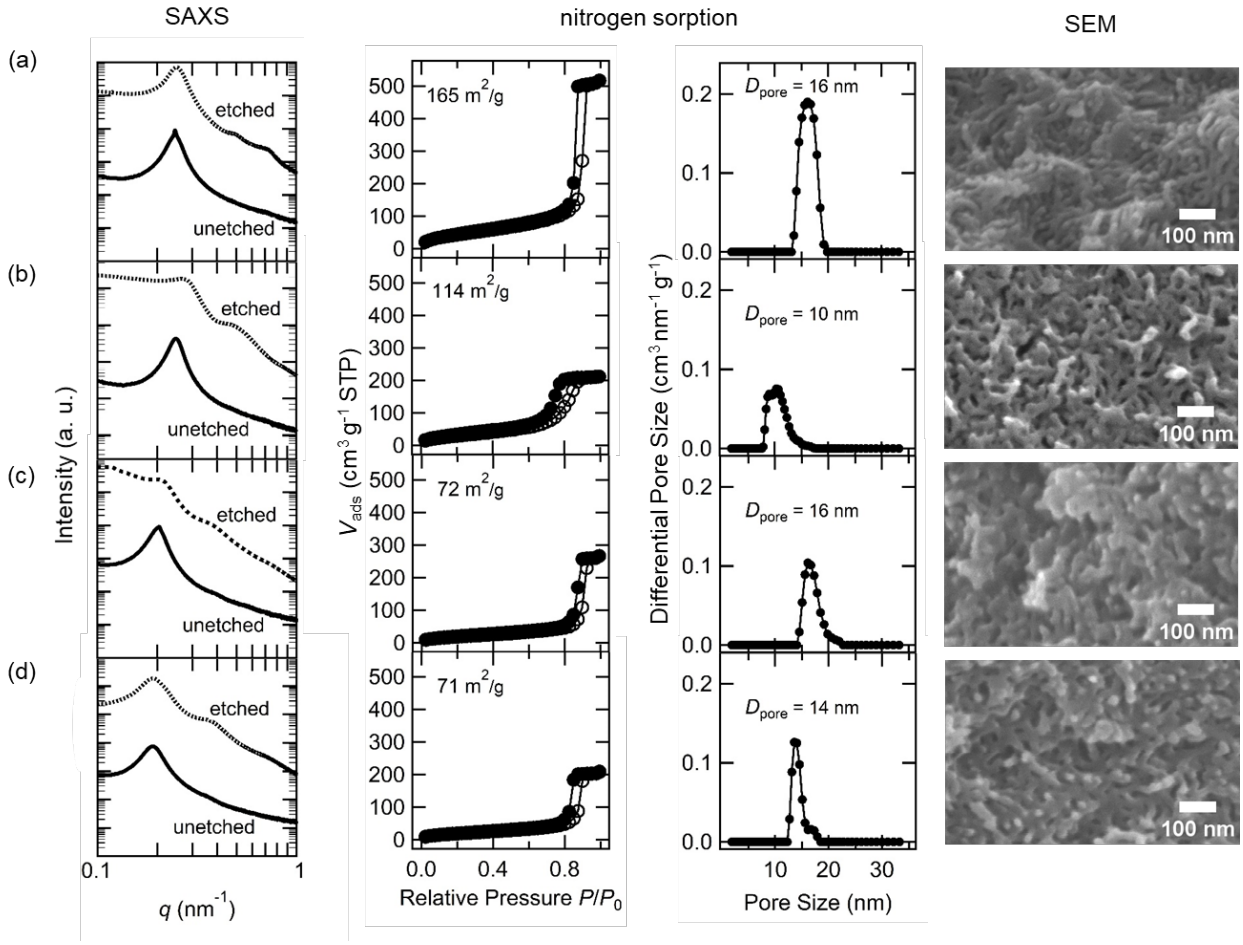

Figure 6. SAXS patterns, nitrogen sorption isotherms, and SEM micrographs for (a) PLA-PSMMA, (b) PLA-POEGMA$_{0.4k}$-PSMMA (c) PLA-POEGMA$_{2.9k}$-PSMMA, and (d) PLA-POEGMA$_{3.0k}$-PSMMA-L. Room temperature SAXS measurements were performed on disordered monoliths before and after selective etching. Nitrogen adsorption (open symbols) and desorption (closed symbols) isotherms were obtained on etched samples. Pore size distributions were obtained from QSDFT analysis. The BET specific surface area and mode pore width for each sample are indicated on the nitrogen sorption plots.

To further characterize the nanoporous structure, nitrogen sorption measurements were performed. Surface area estimated by the Brunauer-Emmett-Teller (BET) method are shown along with the sorption isotherms. BET surface areas range from 70–170 m^2/g, consistent with previous observations on nanoporous disordered monoliths.[24, 27] Notably, the diblock polymer and the triblock with one OEGMA unit at the block junction ($M_{n,\,POEGMA}$ = 0.4 kg/mol) had

noticeably higher surface areas than the triblock polymers. Keeping $M_{n,POEGMA}$ the same while increasing $M_{n,\,PLA}$ and $M_{n,\,PSMMA}$ (PLA-POEGMA$_{2.9k}$-PSMMA vs PLA-POEGMA$_{3.0k}$-PSMMA-L) resulted in similar BET surface areas (Figure 6 c-d). However, further increasing the POEGMA midblock molar mass leads to further decrease in BET surface area and porosity (Table 2, Figure S11). The reduction of surface area post-etching and drying may be due to loss of nanostructure and is consistent with SAXS results (Figure 6), where higher scattering in the low q region relative to the primary scattering peak indicates formation of large features. Changes in nanostructure may be potentially be due to increased plasticization of the matrix when attached to a large POEGMA block, or drying effects. Specific interactions with more polar surfaces can lead to nitrogen molecules adopting a head-on orientation, reducing the cross-sectional area of adsorbed nitrogen and consequently changing the calculated specific surface area.[45] However, this is unlikely to explain the large differences between diblock and triblock materials, and the C constant values are relatively constant across samples, which suggests that the adsorbent-adsorbate interactions are similar (Table 2).[45-46] The N_2 sorption isotherms in Figure 6 show type H1 hysteresis loops, which are associated with mesoporous materials with relatively uniformly distributed pores.[45] Pore size analysis was performed using a quenched solid density functional theory (QSDFT) adsorption branch kernel with a N_2 on carbon, cylindrical pore model.[47] The presented monoliths have monomodal pore size distributions and mode pore widths of ~15 nm, consistent with domain sizes determined by SAXS.

Table 2. Nitrogen sorption and contact angle measurements results. Averages and standard deviations for wetting time and contact angle are reported for at least three replicates.

Sample ID	$f_{midblock}$	BET surface area(m^2/g)[a]	C constant[a]	Wetting time (s)[b]	Monolith water contact angle (°)[b]	Membrane water contact angle (°)[c]
PLA-PSMMA	0	165	41	75 ± 8	87 ± 7	76 ± 2
PLA-POEGMA$_{0.4k}$-PSMMA	0.014	114	33	70 ± 8	87 ± 4	69 ± 3
PLA-POEGMA$_{2.9k}$-PSMMA	0.090	72	39	12 ± 1	63 ± 3	69 ± 2
PLA-POEGMA$_{4.3k}$-PSMMA	0.13	33	33	[d]	[d]	68 ± 3
PLA-POEGMA$_{3.0k}$-PSMMA-L	0.058	71	44	4 ± 1	47 ± 12	64 ± 5
PLA-POEGMA$_{3.5k}$-PS	0.093	[e]	[e]	[e]	[e]	72 ± 5

[a]BET surface area and C constant obtained from nitrogen sorption data. [b] Wetting time and sessile drop water contact angle of dried monoliths measured using a microscopic contact angle instrument, where wetting time was time taken for water droplet deposited on the surface to completely disappear. [c]Water contact angle on composite membranes obtained from captive bubble measurements. [d]Contact angle measurements not performed due to more extensive pore collapse. [e]Nitrogen sorption and microscopic contact angle not performed on the monolith as the ODT is inaccessible in the melt.

Besides heating the triblock polymer melts, the fluctuating disordered state can also be accessed at ambient temperatures through dilution with solvents, which enables the preparation of nanoporous membranes using solution casting methods. Neutral solvents lower T_{ODT}, which allows order-disorder transitions to be observed isothermally by changing solvent concentration.[48-49] Composite membranes comprising selective layers templated by the triblocks were obtained by spin coating the block polymer in chloroform onto pre-formed Nylon membrane supports filled with water followed by etching with 2M NaOH in a water/methanol mixture to remove the PLA domains (Figure S12, S13). The resulting membranes have three dimensionally connected nanopores, with similar disordered morphologies as monoliths

disordered thermally (Figure 6, 7). During spin casting, the block polymer concentration increases due to solvent evaporation and microphase separation occurs. Rapid drying during spin coating leads to vitrification of the block polymers before they have sufficient time to order into thermodynamically favored morphologies, thereby enabling disordered morphologies to be kinetically trapped without the need for thermal annealing steps.[50] Using solution casting methods, the fluctuating disordered state can also be accessed for strongly segregated block polymers with T_{ODT}'s beyond the degradation temperature in the melt. With a PLA-$POEGMA_{3.5k}$-PS triblock, which had no observable T_{ODT} in the melt, nanoporous composite membranes were prepared using the same coating procedure and chloroform as the casting solvent (Figure S14). For the diblock PLA-PS however, casting from chloroform led to poor ordering and low apparent porosity while the use of less volatile toluene led to improved microphase separation (Figure S15).

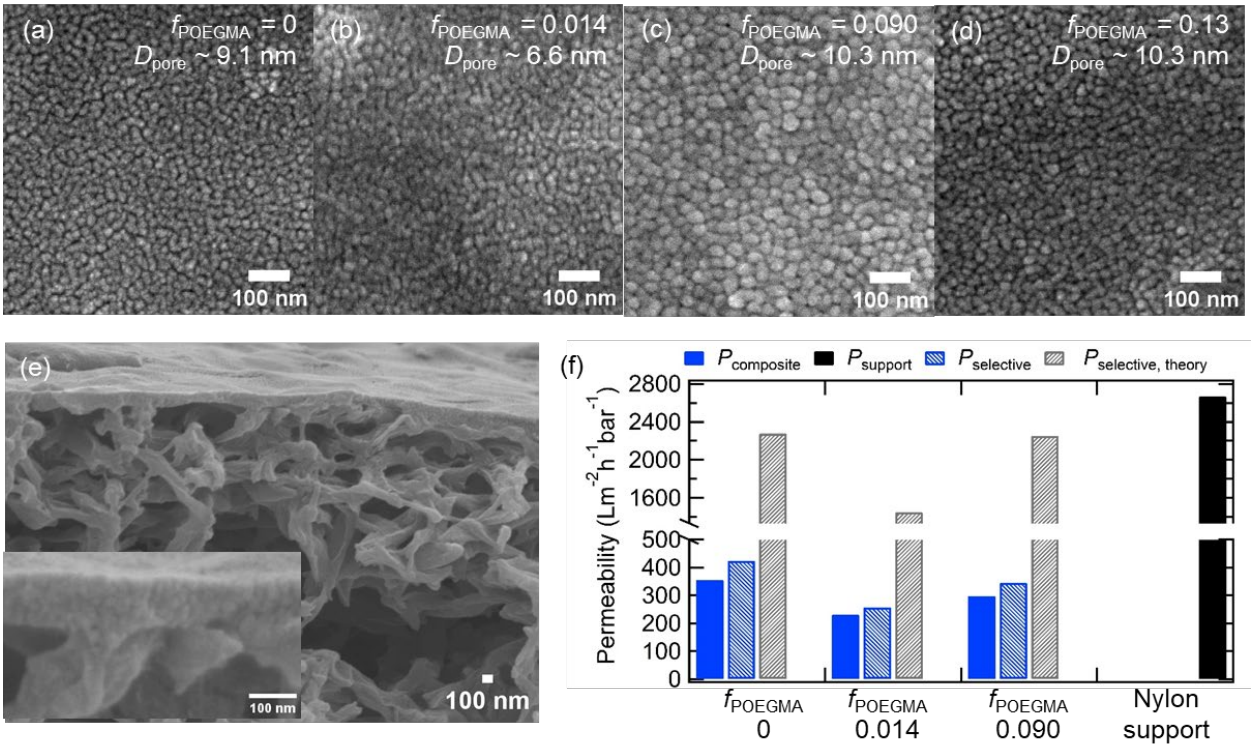

Figure 7. SEM micrographs showing nanopores on composite membranes based on (a) PLA-PSMMA, (b) PLA-POEGMA$_{0.4k}$-PSMMA, (c) PLA-POEGMA$_{2.9k}$-PSMMA, and (d) PLA-POEGMA$_{4.3k}$-PSMMA. Pore sizes were measured from SEM micrographs, averaged across at least 6 measurements. (e) Cross section of PLA-POEGMA$_{0.4k}$-PSMMA membrane. Inset shows the magnified selective layer. (f) Water permeabilities of the Nylon support membrane and composite membranes. Experimental and calculated permeabilities are indicated with solid and hatched bars respectively.

Composite membranes with block polymer selective layers have combined properties of uniform pore sizes and high permeability. Surface pore widths and block polymer layer thicknesses are on the order of 10 nm and 100 nm respectively, as manually estimated from SEM micrographs (Figure 7). After accounting for the 2 nm platinum coating layer deposited for imaging, pore sizes obtained for membranes were consistent with nitrogen sorption and QSDFT analyses on monoliths obtained by quenching disordered melts. For a fixed pore size, permeability scales inversely with membrane thickness. Solution casting onto mechanically robust but highly porous supports, as demonstrated previously,[19, 51] results in thin block polymer coatings of 100–200 nm (Figure 7e),

thereby enabling water high permeabilities of 200–400 L m^{-2} h^{-1} bar^{-1}. These permeabilities are greatly improved when compared to previous work on disordered block polymers cast onto porous membranes (~ 10 L m^{-2} h^{-1} bar^{-1}), [25, 27] potentially due to the elimination of heating steps which can deform the support, and even exceed those of membranes with co-casted selective and support layers (~ 150 L m^{-2} h^{-1} bar^{-1}).[50] The selective layer permeabilities were estimated using a resistors-in-series model which relates the resistance to water flow to the inverse of permeability, P:[52]

$$P_{composite}^{-1} = P_{support}^{-1} + P_{selective}^{-1} \qquad \text{(eq. 2)}$$

where the permeabilities of the composite membranes and the bare Nylon support were measured experimentally. Using these two experimentally determined permeabilities, the estimated values for the selective layer permeabilities are shown in Figure 7f. These values can be compared to the theoretical selective layer permeabilities ($P_{selective,\ theory}$) estimated using the Hagen-Poiseuille equation:

$$P_{selective,theory} = \frac{\varepsilon {r_p}^2}{8\tau^2 \mu \delta_m} \qquad \text{(eq. 3)}$$

where μ is the viscosity of water, porosity (ε) is estimated as the PLA volume fraction, the average pore radius (r_p) was determined from SEM micrographs with 2 nm added to pore sizes to account for the sputter coated platinum layer for imaging, the selective layer thickness (δ_m) was estimated to be ~200 nm from SEM images, and tortuosity (τ) is assumed to be 1.5.[50, 53-54] The membrane based on PLA-POEGMA$_{0.4k}$-PSMMA (f_{POEGMA}: 0.014) has a noticeably smaller permeability than PLA-PSMMA and PLA-POEGMA$_{2.9k}$-PSMMA, likely due to its smaller average pore size. Comparisons between $P_{selective,\ theory}$ and $P_{selective}$ show that permeabilities calculated using experimental measurements are roughly 5–7 times lower than the theoretical values. Deviations may be due to uncertainties in pore radius measurements, which significantly impact permeability

values due to the power of 2 dependence on r_p. Additional factors that may lower permeability include larger tortuosities than expected, smaller effective pore size or porosity from swelling of the pore-lining block, pore collapse, coating defects, or the presence of discontinuous pores.

Incorporation of the POEGMA midblock slightly increased hydrophilicity of the nanoporous materials. To evaluate surface properties of the nanoporous materials, microscopic contact angle measurements were performed on etched and freeze-dried monoliths. The etched diblock PLA-PSMMA is most hydrophobic as it has the highest water contact angles and the longest wetting time, while increasing $M_{n,POEGMA}$ enhanced hydrophilicity (Table 2, Figure S16). The difference in hydrophilicities between diblock and triblock based monoliths provides indirect evidence to the presence of POEGMA on the pore surfaces, even though some degree of interfacial mixing is possible. To evaluate surface properties of composite membranes, captive bubble measurements were performed on never-dried membranes in water (Table 2, Figure S17, see supporting information for membrane preparation details). Marginal improvements in hydrophilicity were observed for membranes with the POEGMA midblock, which decreased the contact angle by ~7° for PLA-POEGMA$_{2.9k}$-PSMMA when compared to PLA-PSMMA. The captive bubble contact angle difference between membranes coated with the diblock and triblocks is smaller when compared to observations made on monoliths, which may be due to drying or skin effects on materials disordered by heating. Increases in hydrophilicity, while marginal, suggest that the midblock is effective at tuning surface properties, and the use of more hydrophilic monomers and longer midblock chain lengths can be explored to further improve membrane surface hydrophilicity.

Deterioration in permeabilities from foulant absorption was observed for both composite and support membranes. Membranes were challenged with bovine serum albumin (BSA) as the

model protein foulant in phosphate buffered saline (PBS, 0.1 M, pH 7.4), and fouling behavior was examined through filtrate flux measurements over time at 0.69 bar and 300 mL/min feed flow rate (Figure 8a). Membranes were first equilibrated with buffer, followed by a switch of the feed to BSA solution. A drastic drop in flux was observed immediately for all membranes, followed by a gradual flux decrease over the course of the fouling experiment (Figure S19). After 4 hours, the membranes were cleaned with PBS at a feed flow rate of 1200 mL/min for at least 20 min, and the filtrate flux re-measured with PBS showed minimal flux recovery for all membranes. The diblock (f_{POEGMA}: 0) and triblock (f_{POEGMA}: 0.09) coated membranes have similar pore sizes and pure water fluxes (Figure S18), but the triblock membrane exhibited higher flux after the switch to PBS and over the course of BSA filtration, which may be an indication of small improvements in fouling resistance for the triblock. However, the large relative flux decreases and small flux recoveries for both diblock and triblock coated membranes suggest that pore-lining POEGMA midblocks have limited effectiveness, or that other factors such as surface roughness or contributions of the Nylon support layer to fouling are dominating. Flux declines during BSA filtration are accompanied by increases in protein rejection. Measurements of BSA concentration in the filtrate (Figure 8b) revealed that the composite membranes were partially retentive to BSA (hydrodynamic radius: 3.3–4.3 nm)[55], consistent with measured pore sizes. BSA rejection increases over the course of the fouling experiment, likely due to the constriction of pores from BSA adsorption and formation of gel polarization layers. On the other hand, the bare Nylon membrane with nominal pore size of 0.1 μm allows the majority of the BSA to permeate through. Unlike the composite membranes, BSA rejection when using bare Nylon supports does not change appreciably in the first 90 min of the filtration experiment, potentially due to the much bigger ratios of pore to BSA radii but does gradually decrease at longer times.

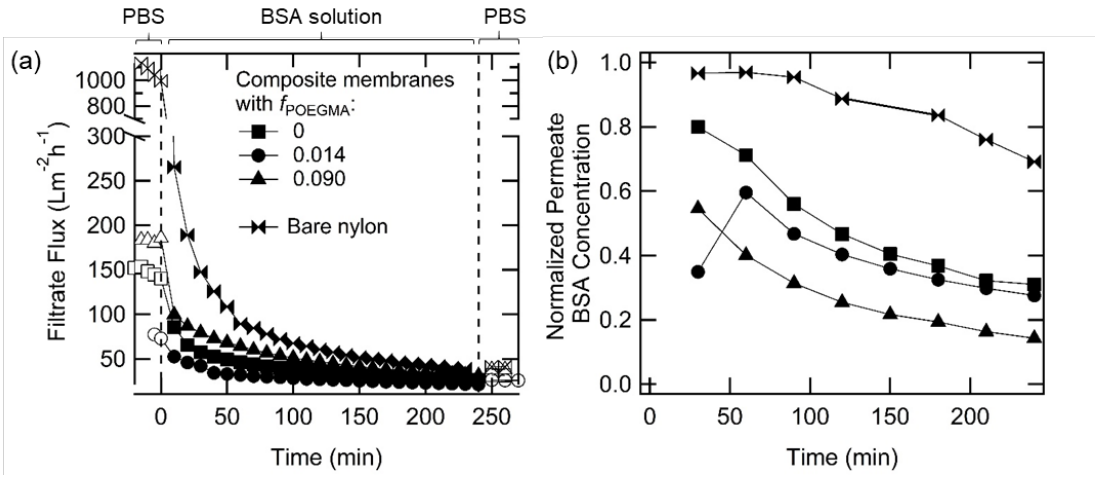

Figure 8. Crossflow filtration of model foulant, BSA (1 g/L in 0.1 M PBS) with bare Nylon and block polymer composite membranes. (a) Filtrate flux measured with 0.1 M PBS buffer (open symbols) and BSA solution (filled symbols) at 0.69 bar. (b) Concentration of BSA in permeate, normalized against starting feed BSA concentration.

The fouling behavior of composite membranes revealed challenges in improving fouling resistance through the coating of a slightly more hydrophilic block polymer layer, within the flow parameters and feed properties investigated. The large flux decline at early times is associated with formation of gel polarization layers, which leads to decreases in permeability and increases in selectivity independent of membrane hydrophilicity.[56-57] On the other hand, flux recovery should be influenced by membrane and solute properties, as hydrophobic membranes will have thicker irreversibly adsorbed layers while the gel polarization layer can be removed by washing. However, limited flux recovery for all membranes, including the bare Nylon support, potentially suggests that the washing step utilized is insufficient for dissolution and removal of the gel layer. In addition, pore plugging may occur due to internal deposition of foulant within pores, which has been observed particularly for microfiltration membranes.[57] Although surface fouling was previously reported to be dominant for UF membranes and the effects of internal

fouling on permeability may be small as the support membrane pores are orders of magnitude larger than BSA,[58] protein adsorption on the inner support membrane pores cannot be conclusively ruled out due to the semi-permeable nature of the selective layer and the high protein binding capacity of Nylon (as indicated by the manufacturer). Uncertainties in contribution of the Nylon support layer on fouling and the effectiveness of washing step therefore complicated the evaluation of the effectiveness of POEGMA pore-lining blocks on fouling resistance, as many other factors can have significant effects on flux declines.

CONCLUSION

Nanoporous materials templated by disordered triblock PLA-POEGMA-PSMMA were investigated, where PLA is the pore-forming etchable block, PSMMA is the matrix block, and POEGMA was selected as the midblock to impart surface hydrophilicity to the materials. Fluctuating disordered triblocks were obtained by heating polymer melts above the T_{ODT} followed by quenching, or by rapidly evaporating solvent from polymer solutions during solution casting at room temperature. Presence of accessible T_{ODT}'s in the melt is highly dependent on segregation strengths of the end blocks, $\chi_{PLA\text{-}PSMMA}N$, which can be tuned by changing the percent styrene in the PSMMA block or the total degree of polymerization. Due to the high compatibility between POEGMA/PLA, the POEGMA block is expected to co-localize with the PLA domain, although some level of interfacial mixing with PSMMA is likely. After selective removal of PLA by selective etching, nanoporous materials with uniform pore sizes were obtained in both block polymer monoliths and composite membranes with 100–200 nm thick block polymer coatings. Composite membranes with the disordered block polymer selective

layers were obtained without the need for heating or any annealing steps, and were demonstrated to have high permeabilities in the range of 200–400 L m^{-2} h^{-1} bar^{-1}. POEGMA in the triblocks lowered water contact angles and decreased wetting time for monoliths, and provided marginal improvements in hydrophilicity for composite membranes (7–12° decrease in water contact angle). The composite membranes however, were still prone to protein fouling within the crossflow filtration conditions tested. This work therefore demonstrates the use of triblock polymers as a strategy for designing membranes with tunable surface properties, where the kinetic trapping of the fluctuating disordered morphology allows three dimensionally connected and uniform nanopores to be obtained using straightforward solution casting methods. Further improvements in membrane surface hydrophilicity, however, will likely require more hydrophilic monomers or larger midblocks, and further investigations on the role of support layer in fouling and the mechanism of fouling as a function of pore size, solute rejection, surface roughness will be needed to evaluate the effectiveness of hydrophilic isoporous selective layers on composite membranes.

ASSOCIATED CONTENT

Supporting Information. Experimental details. ^{1}H NMR and SEC traces for PLA-CTA, diblock PLA-POEGMA, and triblock PLA-POEGMA-PSMMA. Molecular details for all triblock polymers, DSC measurement on POEGMA/PSMMA blend, rheology measurements, SEM micrographs of triblocks with increasing POEGMA fraction, SEC traces for POEGMA incubated in etching solution, etching condition screening, SEM micrographs of triblocks after methanol

plasticization, ATR-FTIR spectra for composite membranes, images of droplets for measuring water contact angle on monoliths, flux measurements for composite membranes.

AUTHOR INFORMATION

Corresponding Author

Email: hillmyer@umn.edu

Author Contributions

The manuscript was written through contributions of all authors. All authors have given approval to the final version of the manuscript.

Funding Sources

Funding for this work was provided by the National Science Foundation (DMR-2003454) and the University of Minnesota President's Postdoctoral Fellowship Program.

ACKNOWLEDGMENT

Portions of this work were performed at the DuPont-Northwestern-Dow Collaborative Access Team (DND-CAT) located at the Sector 5 of the Advanced Photon Source (APS). DND-CAT is supported by E.I. DuPont de Nemours & Co., the Dow Chemical Company, and Northwestern University. Use of the APS, an Office of Science User Facility operated for the U.S. DOE Office of Science by Argonne National Laboratory, was supported by the U.S. DOE under contract no. DE-AC02-06CH11357.The authors are extremely grateful to Steven Weigand for help with collecting SAXS data. SEM and microscopic contact angle data was collected at the UMN Characterization Facility, which receives partial support from NSF through the MRSEC

program. The authors would like to thank Nicholas Hampu and Jay Werber for reviewing the manuscript.

REFERENCES

1. Guillen, G. R.; Pan, Y. J.; Li, M. H.; Hoek, E. M. V., Preparation and Characterization of Membranes Formed by Nonsolvent Induced Phase Separation: A Review. *Industrial & Engineering Chemistry Research* **2011,** *50* (7), 3798-3817,10.1021/ie101928r.
2. Hampu, N.; Werber, J. R.; Chan, W. Y.; Feinberg, E. C.; Hillmyer, M. A., Next-Generation Ultrafiltration Membranes Enabled by Block Polymers. *Acs Nano* **2020,** *14* (12), 16446-16471
3. Hester, J. F.; Banerjee, P.; Mayes, A. M., Preparation of protein-resistant surfaces on poly(vinylidene fluoride) membranes via surface segregation. *Macromolecules* **1999,** *32* (5), 1643-1650,DOI 10.1021/ma980707u.
4. Hester, J. F.; Mayes, A. M., Design and performance of foul-resistant poly(vinylidene fluoride) membranes prepared in a single-step by surface segregation. *J Membrane Sci* **2002,** *202* (1-2), 119-135,Pii S0376-7388(01)00735-9

Doi 10.1016/S0376-7388(01)00735-9.
5. Zhang, Y. Z.; Sargent, J. L.; Boudouris, B. W.; Phillip, W. A., Nanoporous membranes generated from self-assembled block polymer precursors: Quo Vadis? *Journal of Applied Polymer Science* **2015,** *132* (21),ARTN 41683

10.1002/app.41683.
6. Zhang, Y.; Almodovar-Arbelo, N. E.; Weidman, J. L.; Corti, D. S.; Boudouris, B. W.; Phillip, W. A., Fit-for-purpose block polymer membranes molecularly engineered for water treatment. *npj Clean Water* **2018,** *1* (1), 1-14
7. Nunes, S. P., Block copolymer membranes for aqueous solution applications. *Macromolecules* **2016,** *49* (8), 2905-2916
8. Zhou, J. M.; Wang, Y., Selective Swelling of Block Copolymers: An Upscalable Greener Process to Ultrafiltration Membranes? *Macromolecules* **2020,** *53* (1), 5-17
9. Wang, Y., Nondestructive Creation of Ordered Nanopores by Selective Swelling of Block Copolymers: Toward Homoporous Membranes. *Accounts Chem Res* **2016,** *49* (7), 1401-1408
10. Phillip, W. A.; O'Neill, B.; Rodwogin, M.; Hillmyer, M. A.; Cussler, E. L., Self-Assembled Block Copolymer Thin Films as Water Filtration Membranes. *Acs Appl Mater Inter* **2010,** *2* (3), 847-853,10.1021/am900882t.
11. Yang, S. Y.; Park, J.; Yoon, J.; Ree, M.; Jang, S. K.; Kim, J. K., Virus filtration membranes prepared from nanoporous block copolymers with good dimensional stability under high pressures and excellent solvent resistance. *Adv Funct Mater* **2008,** *18* (9), 1371-1377
12. Mao, H.; Hillmyer, M. A., Nanoporous polystyrene by chemical etching of poly (ethylene oxide) from ordered block copolymers. *Macromolecules* **2005,** *38* (9), 4038-4039

13. Satoh, K.; Poelma, J. E.; Campos, L. M.; Stahl, B.; Hawker, C. J., A facile synthesis of clickable and acid-cleavable PEO for acid-degradable block copolymers. *Polym Chem-Uk* **2012,** *3* (7), 1890-1898
14. Dorin, R. M.; Sai, H.; Wiesner, U., Hierarchically Porous Materials from Block Copolymers. *Chem Mater* **2014,** *26* (1), 339-347,10.1021/cm4024056.
15. Abetz, V., Isoporous Block Copolymer Membranes. *Macromol Rapid Comm* **2015,** *36* (1), 10-22
16. Peinemann, K. V.; Abetz, V.; Simon, P. F. W., Asymmetric superstructure formed in a block copolymer via phase separation. *Nature Materials* **2007,** *6* (12), 992-996
17. Yang, H.; Wang, Z.; Lan, Q.; Wang, Y., Antifouling ultrafiltration membranes by selective swelling of polystyrene/poly (ethylene oxide) block copolymers. *J Membrane Sci* **2017,** *542*, 226-232
18. Mao, H.; Arrechea, P. L.; Bailey, T. S.; Johnson, B. J.; Hillmyer, M. A., Control of pore hydrophilicity in ordered nanoporous polystyrene using an AB/AC block copolymer blending strategy. *Faraday Discuss* **2005,** *128*, 149-162
19. Querelle, S. E.; Jackson, E. A.; Cussler, E. L.; Hillmyer, M. A., Ultrafiltration membranes with a thin poly (styrene)-b-poly (isoprene) selective layer. *Acs Appl Mater Inter* **2013,** *5* (11), 5044-5050
20. Rzayev, J.; Hillmyer, M. A., Nanoporous polystyrene containing hydrophilic pores from an ABC triblock copolymer precursor. *Macromolecules* **2005,** *38* (1), 3-5
21. Bailey, T. S.; Rzayev, J.; Hillmyer, M. A., Routes to alkene and epoxide functionalized nanoporous materials from poly(styrene-b-isoprene-b-lactide) triblock copolymers. *Macromolecules* **2006,** *39* (25), 8772-8781,10.1021/ma061892b.
22. Shevate, R.; Karunakaran, M.; Kumar, M.; Peinemann, K. V., Polyanionic pH-responsive polystyrene-b-poly(4-vinyl pyridine-N-oxide) isoporous membranes. *J Membrane Sci* **2016,** *501*, 161-168,10.1016/j.memsci.2015.11.038.
23. Lee, S.; Gillard, T. M.; Bates, F. S., Fluctuations, Order, and Disorder in Short Diblock Copolymers. *Aiche J* **2013,** *59* (9), 3502-3513
24. Hampu, N.; Hillmyer, M. A., Molecular Engineering of Nanostructures in Disordered Block Polymers. *Acs Macro Lett* **2020,** *9* (3), 382-388,10.1021/acsmacrolett.0c00036.
25. Hampu, N.; Hillmyer, M. A., Temporally Controlled Curing of Block Polymers in the Disordered State Using Thermally Stable Photoacid Generators for the Preparation of Nanoporous Membranes. *Acs Appl Polym Mater* **2019,** *1* (5), 1148-1154,10.1021/acsapm.9b00150.
26. Hampu, N.; Bates, M. W.; Vidil, T.; Hillmyer, M. A., Bicontinuous Porous Nanomaterials from Block Polymers Radically Cured in the Disordered State for Size-Selective Membrane Applications. *Acs Appl Nano Mater* **2019,** *2* (7), 4567-4577,10.1021/acsanm.9b00922.
27. Vidil, T.; Hampu, N.; Hillmyer, M. A., Nanoporous Thermosets with Percolating Pores from Block Polymers Chemically Fixed above the Order-Disorder Transition. *Acs Central Sci* **2017,** *3* (10), 1114-1120,10.1021/acscentsci.7b00358.
28. Jang, H.; Song, D. H.; Kim, I. C.; Kwon, Y. N., Fouling control through the hydrophilic surface modification of poly(vinylidene fluoride) membranes. *Journal of Applied Polymer Science* **2015,** *132* (21),ARTN 41712

10.1002/app.41712.

29. Asatekin, A.; Kang, S.; Elimelech, M.; Mayes, A. M., Anti-fouling ultrafiltration membranes containing polyacrylonitrile-graft-poly (ethylene oxide) comb copolymer additives. *J Membrane Sci* **2007,** *298* (1-2), 136-146,10.1016/j.memsci.2007.04.011.
30. Akthakul, A.; Salinaro, R. F.; Mayes, A. M., Antifouling polymer membranes with subnanometer size selectivity. *Macromolecules* **2004,** *37* (20), 7663-7668,10.1021/ma048837s.
31. Asatekin, A.; Olivetti, E. A.; Mayes, A. M., Fouling resistant, high flux nanofiltration membranes from polyacrylonitrile-graft-poly(ethylene oxide). *J Membrane Sci* **2009,** *332* (1-2), 6-12,10.1016/j.memsci.2009.01.029.
32. Rosedale, J. H.; Bates, F. S.; Almdal, K.; Mortensen, K.; Wignall, G. D., Order and disorder in symmetric diblock copolymer melts. *Macromolecules* **1995,** *28* (5), 1429-1443
33. Hickey, R. J.; Gillard, T. M.; Lodge, T. P.; Bates, F. S., Influence of Composition Fluctuations on the Linear Viscoelastic Properties of Symmetric Diblock Copolymers near the Order-Disorder Transition. *Acs Macro Lett* **2015,** *4* (2), 260-265
34. Baiardo, M.; Frisoni, G.; Scandola, M.; Rimelen, M.; Lips, D.; Ruffieux, K.; Wintermantel, E., Thermal and mechanical properties of plasticized poly(L-lactic acid). *Journal of Applied Polymer Science* **2003,** *90* (7), 1731-1738
35. Sheth, M.; Kumar, R. A.; Dave, V.; Gross, R. A.; McCarthy, S. P., Biodegradable polymer blends of poly(lactic acid) and poly(ethylene glycol). *Journal of Applied Polymer Science* **1997,** *66* (8), 1495-1505,Doi 10.1002/(Sici)1097-4628(19971121)66:8<1495::Aid-App10>3.0.Co;2-3.
36. Gaikwad, A. N.; Wood, E. R.; Ngai, T.; Lodge, T. P., Two calorimetric glass transitions in miscible blends containing poly (ethylene oxide). *Macromolecules* **2008,** *41* (7), 2502-2508
37. Neumann, C.; Abetz, V.; Stadler, R., Phase behavior of ABC-triblock copolymers with two inherently miscible blocks. *Colloid Polym Sci* **1998,** *276* (1), 19-27
38. Neumann, C.; Loveday, D.; Abetz, V.; Stadler, R., Morphology, dynamic mechanical properties, and phase behavior of ABC-triblock copolymers with two semicompatible elastomer blocks. *Macromolecules* **1998,** *31* (8), 2493-2500
39. Kennemur, J. G.; Yao, L.; Bates, F. S.; Hillmyer, M. A., Sub-5 nm Domains in Ordered Poly(cyclohexylethylene)-block-poly(methyl methacrylate) Block Polymers for Lithography. *Macromolecules* **2014,** *47* (4), 1411-1418
40. Zalusky, A. S.; Olayo-Valles, R.; Wolf, J. H.; Hillmyer, M. A., Ordered nanoporous polymers from polystyrene-polylactide block copolymers. *Journal of the American Chemical Society* **2002,** *124* (43), 12761-12773,10.1021/ja0278584.
41. Wylie, K.; Dong, L.; Chandra, A.; Nabae, Y.; Hayakawa, T., Modifying the Interaction Parameters of a Linear ABC Triblock Terpolymer by Functionalizing the Short, Reactive Middle Block To Induce Morphological Change. *Macromolecules* **2020,** *53* (4), 1293-1301,10.1021/acs.macromol.9b02567.
42. Werner, A.; Fredrickson, G. H., Architectural effects on the stability limits of ABC block copolymers. *J Polym Sci Pol Phys* **1997,** *35* (5), 849-864
43. Schönemann, E.; Laschewsky, A.; Rosenhahn, A., Exploring the long-term hydrolytic behavior of zwitterionic polymethacrylates and polymethacrylamides. *Polymers-Basel* **2018,** *10* (6), 639
44. Han, M.-J.; Bhattacharyya, D., Thermal annealing effect on cellulose acetate reverse osmosis membrane structure. *Desalination* **1995,** *101* (2), 195-200
45. Thommes, M., Physical adsorption characterization of nanoporous materials. *Chemie Ingenieur Technik* **2010,** *82* (7), 1059-1073

46. Trens, P.; Denoyel, R.; Glez, J. C., Comparative adsorption of argon and nitrogen for the characterisation of hydrophobized surfaces. *Colloids and Surfaces A: Physicochemical and Engineering Aspects* **2004,** *245* (1-3), 93-98
47. Landers, J.; Gor, G. Y.; Neimark, A. V., Density functional theory methods for characterization of porous materials. *Colloids and Surfaces A: Physicochemical and Engineering Aspects* **2013,** *437*, 3-32
48. Lodge, T. P.; Hanley, K. J.; Pudil, B.; Alahapperuma, V., Phase behavior of block copolymers in a neutral solvent. *Macromolecules* **2003,** *36* (3), 816-822
49. Baruth, A.; Seo, M.; Lin, C. H.; Walster, K.; Shankar, A.; Hillmyer, M. A.; Leighton, C., Optimization of long-range order in solvent vapor annealed poly (styrene)-block-poly (lactide) thin films for nanolithography. *Acs Appl Mater Inter* **2014,** *6* (16), 13770-13781
50. Hampu, N.; Werber, J. R.; Hillmyer, M. A., Co-Casting Highly Selective Dual-Layer Membranes with Disordered Block Polymer Selective Layers. *Acs Appl Mater Inter* **2020,** *12* (40), 45351-45362
51. Wang, Y.; Zhang, C.; Zhou, J.; Wang, Y., Room-temperature swelling of block copolymers for nanoporous membranes with well-defined porosities. *J Membrane Sci* **2020,** *608*, 118186
52. Henis, J. M. S.; Tripodi, M. K., Composite Hollow Fiber Membranes for Gas Separation - the Resistance Model Approach. *J Membrane Sci* **1981,** *8* (3), 233-246,Doi 10.1016/S0376-7388(00)82312-1.
53. Epstein, N., On tortuosity and the tortuosity factor in flow and diffusion through porous media. *Chem Eng Sci* **1989,** *44* (3), 777-779
54. Li, L.; Schulte, L.; Clausen, L. D.; Hansen, K. M.; Jonsson, G. E.; Ndoni, S., Gyroid nanoporous membranes with tunable permeability. *ACS nano* **2011,** *5* (10), 7754-7766
55. Jachimska, B.; Wasilewska, M.; Adamczyk, Z., Characterization of globular protein solutions by dynamic light scattering, electrophoretic mobility, and viscosity measurements. *Langmuir* **2008,** *24* (13), 6866-6872
56. Cherkasov, A.; Tsareva, S.; Polotsky, A., Selective properties of ultrafiltration membranes from the standpoint of concentration polarization and adsorption phenomena. *J Membrane Sci* **1995,** *104* (1-2), 157-164
57. Marshall, A.; Munro, P.; Trägårdh, G., The effect of protein fouling in microfiltration and ultrafiltration on permeate flux, protein retention and selectivity: a literature review. *Desalination* **1993,** *91* (1), 65-108
58. Jim, K.; Fane, A.; Fell, C.; Joy, D.] Fouling mechanisms of membranes during protein ultrafiltration. *J Membrane Sci* **1992,** *68* (1-2), 79-91